Applied Catalysis B: Environmental 91 (2009) 83–91

Contents lists available at ScienceDirect

Applied Catalysis B: Environmental

journal homepage: www.elsevier.com/locate/apcatb

Controlled synthesis of Pt-Sn/C fuel cell catalysts with exclusive Sn–Pt interaction Application in CO and ethanol electrooxidation reactions

Sergio García-Rodríguez [a], Ferenc Somodi [b], Irina Borbáth [b], József L. Margitfalvi [b], Miguel Antonio Peña [a], Jose Luis G. Fierro [a], Sergio Rojas [a,*]

[a] Estructura y Reactividad de Catalizadores, Instituto de Catálisis y Petroleoquímica, CSIC C/Marie Curie 2, 28049, Madrid, Spain
[b] Institute of Nanochemistry and Catalysis, Chemical Research Center, HAS, POB 17, 1525 Budapest, Hungary

ARTICLE INFO

Article history:
Received 9 February 2009
Received in revised form 3 May 2009
Accepted 10 May 2009
Available online 19 May 2009

Keywords:
PtSn/C electrocatalysts
Controlled surface reactions
Pt_3Sn
Sn–Pt interaction
Ethanol
Electrooxidation

ABSTRACT

A series of Sn modified carbon supported Pt electrocatalysts displaying an increasing amount of the Pt_3Sn crystalline phase within their structure has been prepared by using controlled surface reactions (CSRs). This synthetic route results in the exclusive incorporation of Sn onto the Pt sites yielding $Pt_{(1-x)}Sn_x$ and Pt_3Sn phases. As demonstrated by X-ray diffraction and transmission electron microscopy the amount of the Pt_3Sn phase within the electrocatalysts can be controlled by tuning the reaction conditions in CSRs. CO and ethanol electrooxidation reactions were studied over these new type of Sn-Pt/C catalysts, demonstrating that the presence of the Pt_3Sn structure effectively facilitates both processes, particularly the ethanol electrooxidation.

© 2009 Elsevier B.V. All rights reserved.

1. Introduction

Direct alcohol fuel cells are devices that can extract the chemical energy accumulated in molecules such as hydrogen, methanol or ethanol producing electrical work [1].

Direct methanol fuel cells (DMFCs) are the most developed technology; however, ethanol is regarded as the most attractive fuel since it can be obtained in a sustainable way, easily stored and transported and is less harmful than methanol [2,3]. A serious drawback to the implementation of this technology is the lack of efficient ethanol oxidation electrocatalysts [4]. Such catalysts should combine high tolerance to CO together with the ability to break the C–C bond under mild conditions. This is not possible with the state of the art Pt catalysts. However, by forming bimetallic catalysts it is possible to modify the electronic and structural properties of Pt, hence improving its catalytic performance by favoring the desired reaction pathway. With the aim of improving its performance towards ethanol electrooxidation Pt has been modified among others with Ru, W, Ir, Sn [5,6]. Among the plethora of bimetallic electrocatalysts under study, PtSn-based ones appear as the most promising approach [7–10]. There is a large body of work describing the enhanced CO and methanol electrooxidation on well characterized Sn modified Pt($h\,k\,l$) surfaces [11] pinpointing the predominant role of the Pt_3Sn phase in either reaction. This is not straightforward demonstrated for actual carbon supported tin modified platinum electrocatalysts. One reason can be that the synthesis of nano-sized Pt-Sn particles of a controlled composition is still complicated [8,9,12,13]. Most synthetic routes lead to solids with a wide range of phases such as Pt, either reduced or as oxide, Sn oxides or Pt-Sn solid solutions all of which contain isolated tin oxide phases [14]. Generally, synthetic routes for the preparation of Pt-Sn solids involve colloidal techniques or solid state reactions followed by thermal treatment in order to form the, in principle desired Pt_3Sn alloy [15–21].

The exclusive formation of supported Sn–Pt alloy phases with different Pt/Sn ratios can be achieved by using controlled surface reactions (CSRs) between hydrogen adsorbed on Pt sites and tin tetraalkyls [22–24]. For instance, Sn-Pt/SiO_2 catalysts synthesized by means of CSRs display high activity in CO oxidation [24]. Also, the synthesis of carbon supported PtSn electrocatalysts has been undertaken by means of surface organometallic chemistry [25].

This manuscript describes a modification of the controlled surface reaction synthesis of Sn modified carbon supported Pt electrocatalysts with the aim to synthesizing electrocatalysts of controlled Pt/Sn ratios displaying different content of the Pt_3Sn phase. The performance of the new type of Sn-Pt/C electrocatalysts has been evaluated in CO and ethanol electrooxidation reactions.

* Corresponding author. Tel.: +34 91 585 4937; fax: +34 91 585 4760.
E-mail address: srojas@icp.csic.es (S. Rojas).

0926-3373/$ – see front matter © 2009 Elsevier B.V. All rights reserved.
doi:10.1016/j.apcatb.2009.05.009

A clear correlation between Pt_3Sn content and the electrocatalytic performance has also been established.

2. Experimental

2.1. Synthesis of Sn modified Pt/C catalysts

The general approach for the synthesis of the Sn modified supported Pt catalysts by using controlled surface reaction has been described earlier as a two step anchoring type surface reaction. Upon using tetraethyltin these reactions can be written as follows [26,27]:

$$PtH_{ads.} + Sn(C_2H_5)_4 \rightarrow Pt\text{-}Sn(C_2H_5)_{(4-x)} + xC_2H_6 \quad (1)$$

$$Pt\text{-}Sn(C_2H_5)_{(4-x)} + (4-x)/2H_2 \rightarrow Pt - Sn + (4-x)C_2H_6 \quad (2)$$

In the first step of tin anchoring tetraethyltin reacts with hydrogen adsorbed on platinum resulting in ethane and primary surface complexes (PSC) with general formula of $Pt\text{-}Sn(C_2H_5)_{(4-x)}$ (see reaction (1)). In a subsequent step (reaction (2)) the PSC are decomposed in hydrogen resulting in supported alloy-type Sn–Pt nano-clusters. The use of the above approach gives a definite guaranty for the exclusive introduction of tin onto platinum, i.e. for the suppression of tin-support interaction.

A parent Pt/C catalyst (Johnson Matthey, 40 wt.%) and tetraethyltin ($Sn(C_2H_5)_4$) (Fluka) was used to prepare tin modified Pt/C electrocatalysts. Prior to the tin anchoring step (reaction (1)) the parent Pt/C catalyst was re-reduced in flowing H_2 (at 350 °C for 2 h) and transferred into a glass reactor without exposure to air and slurred with deoxygenated solvent (*n*-heptane at T_r = 20–80 °C or *n*-decane at T_r = 120 °C). Upon reaching the required reaction temperature the reactor was filled with hydrogen and the tin anchoring reaction was started by the injection of appropriate amount of $Sn(C_2H_5)_4$ into the slurry. The reaction was monitored by gas chromatography (equipped with a 3 m Al_2O_3 column and operating at 100 °C) to determine the amount of ethane formed. When the increase of the amount of ethane formed was practically stopped, the reactor was purged with argon, evacuated and filled again with hydrogen, creating in these way additional periods in the first step of tin anchoring. In some cases (see Sn_0/Pt values in Table 1) new portion of $Sn(C_2H_5)_4$ was also added. When the tin anchoring step was completed, the catalyst was washed with pure solvent and dried in vacuum for 2 h.

The decomposition of formed $Pt\text{-}Sn(C_2H_5)_{(4-x)}$ surface complexes (reaction (2)) was carried out in H_2 atmosphere by the temperature programmed decomposition technique (experimental parameters: heating interval = 25–350 °C, heating rate = 5 °C/min, hydrogen flow rate = 30 ml/min, amount of catalyst = 0.2 g). The total amount of ethane formed during tin anchoring step (reaction (1)) can be calculated as the sum of the amounts of ethane formed in each period ($n_t^I = \sum n^I$). The sum of the amount of ethane formed during reaction (1) (n_t^I, mol/g_{cat}) and reaction (2) (n^{II}, mol/g_{cat}) allowed obtaining full material balance of tin anchoring. Based on the overall material balance the stoichiometry of tin anchoring step (1), i.e., the value of x ($x = 4n_t^I/(n_t^I + n^{II})$, was calculated.

Three samples with different Sn loading were obtained. Samples were labeled as PtSn-L, PtSn-M and PtSn-H for the low, medium and high Sn loading, respectively. As shown below, the nomenclature also applies to the increasing content of the Pt_3Sn phase in the electrocatalysts.

2.2. Physicochemical and electrochemical characterization

X-ray diffraction (XRD) analysis was performed using an X-ray diffractometer from X'Pert Pro PANalytical. 2θ scans 2 and 90° with 0.04°/step and a count time per step of 20 s. Selected 2θ regions were recorded during 500 s in order to magnify the intensity of the desired reflections by enhancing the signal to noise ratio.

Transmission electron microscope (TEM) images were recorded in a JEOL microscope model JEM-2100F. Specimens for analysis were dispersed in ethanol in an ultrasonic bath and few drops were deposited over a 200 mesh copper lacey carbon grid from SPI. EDX analysis was performed in an Oxford INCAx-Sight EDS detector and an INCAEnergy software package.

X-ray photoelectron spectra (XPS) were acquired with a VG Escalab 200R spectrometer fitted with Mg 120 W X-ray source. Samples were placed in a pretreatment chamber, degassed at room temperature and 10^{-5} mbar for 5 h prior to transfer to the analysis chamber. Residual pressure during the analysis was maintained below 3×10^{-9} mbar. Intensities were estimated by calculating the integral of each peak, determined by subtraction of the Shirley type background and fitting of the experimental curve to a combination of Lorentzian and Gaussian lines. Accurate binding energies (±0.2 eV) were determined by referencing to the C 1s peak at 284.6 eV.

Electrochemical studies were carried out at 25 °C in a thermostated conventional three-compartment electrochemical glass cell. A glassy carbon rotating disk electrode (0.283 cm^2, GC-Typ zu628) was used as a substrate for the catalyst. Unless otherwise stated, current densities are referred to the geometric

Table 1
General data related to tin anchoring.

N°	Periods of step (1)	Solvent	T_rC	Sn_0/Pt[a]	Time (h)	$W_0 \times 10^{-6}$[b]	$n^I \times 10^{-6}$[c]	$n^{II} \times 10^{-6}$[d]	x	Sn (wt.%)[e]	Sn/Pt
PtSn-L	1st	C_7H_{16}	70	0.5	3.5	105.9	398.3				
	2nd		70	–	3.5	2.5	184.3	54.8	3.66	1.9	0.08
PtSn-M	1st	C_7H_{16}	20	1.7	20	147.8	456.6				
	2nd		70	–	2	31.4	283.3				
	3rd		70	–	5	5.8	240.1	47.1	3.87	4.3	0.18
	4th		80	0.9	7	4.0	406.0				
PtSn-H	1st	$C_{10}H_{22}$	120	0.9	2	359.0	1122.8				
	2nd		120	0.9	5	14.3	309.8				
	3rd		120	0.9	5	7.4	319.6	83.2	3.84	6.2	0.25
	4th		120	0.9	5	6.9	235.7				

Amount of the Pt/C catalyst: 0.5 g; atmosphere of tin anchoring: H_2.
[a] Amount of $Sn(C_2H_5)_4$ per one Pt injected at the beginning of a given period of tin anchoring step (1).
[b] Initial rate of tin anchoring reaction of a given period in step (1), (mol/(g_{cat} *x* min).
[c] Amount of ethane formed during a given period of tin anchoring step (1) (mol/g_{cat}).
[d] Amount of ethane formed in step (2) (mol/g_{cat}).
[e] Tin content calculated from the material balance of tin anchoring.

area of the electrode. Previous to each test, the electrode was polished with alumina 0.05 μm to obtain a mirror finish, and it was rinsed with triply distilled water in an ultrasonic bath. An Ag/AgCl 3 M KCl electrode and a platinum wire as the reference and the counter electrodes were used. In the manuscript, all potentials are referred to the normal hydrogen electrode (NHE).The samples under study were deposited onto the working electrode by means of an ink [28]. Typically, 5 mg of the electrocatalyst, 30 μL of 5 wt.% of Nafion solution (Aldrich), and 700 μL of Mili-Q water were dispersed in an ultrasonic bath for 45 min, obtaining a homogenous ink. 20 μL of the ink were dropped onto the electrode and dried at room temperature resulting in a homogenous coating. This leads to a final Pt loading of 194 μg Pt cm^{-2}. A 0.5 M H_2SO_4 water solution (Merck) was used as the electrolyte. All solutions were prepared with Mili-Q water. Electrochemical measurements were performed with a computer controlled potentiostat/galvanostat EG&G 273A.

3. Results and discussion

3.1. Preparation of PtSn/C electrocatalysts

Experimental results related to tin anchoring onto the parent Pt/C catalyst are summarized in Table 1. The main goal of these experiments was to get a series of alloy type PtSn/C catalysts with different tin content. The key experimental variables (see Table 1) were as follows: (i) initial concentration of $Sn(C_2H_5)_4$ (Sn_o/Pt ratio); (ii) temperature of tin anchoring reaction (T_r), and (iii) duration of tin anchoring.

The samples PtSn-L and PtSn-H with the lowest and highest tin content were obtained at T_r = 70 °C and T_r = 120 °C, respectively and the preparation consisted of two and four consecutive tin anchoring periods as shown in Fig. 1A and B. As it was expected in both cases the highest initial rate of tin anchoring was observed during the first period over the fresh Pt/C catalyst. As it is shown in Fig. 1A in the course of preparation of PtSn-L catalyst in the first period of tin anchoring the formation of ethane is almost ceased after 50 min however, after the addition of new portion of hydrogen surface reaction (1) was restarted again. In this way the amount of tin anchored could be increased. This approach appeared to be useful in all other experiments as shown in Fig. 1B. However, at 120 °C further increase of the amount of tin anchored required three additional periods. In these periods new portions of tetraethyltin were also introduced (see Table 1).

The results given in Table 1 unambiguously show that upon using surface reactions (1) and (2) the tin content of the catalysts varied in the range of 1.9–6.2 wt.%. High reaction temperature (T_r), high Sn_o/Pt ratio and increased reaction time favor the increase of the tin content.

In our earlier studies [29], it has been demonstrated that the use of both the increased reaction temperature and hydrogen atmosphere strongly influences both the rate of tin anchoring and the amount of alkyl groups left in PSC in surface reaction (1). It has to be emphasized that in the first step of tin anchoring the extent of loss of ethyl groups is extremely high (see values of x given in Table 1 (x = the number of alkyl groups per one tin atom lost in surface reaction (1)). The mean value of x is 3.79. It means that around 95% of the ethyl groups in $Sn(C_2H_5)_4$ reacted in the first step of tin anchoring. Consequently, in surface reaction (1) "naked" Sn (x = 4.0) over Pt is forming in high abundance. In this form tin present as adatoms on the surface of platinum atoms and is transformed to platinum–tin alloy in surface reaction (2). Moreover, the high values of x can also indicate that the modification of Pt with Sn using CSRs is highly selective.

3.2. Physicochemical characterization

Fig. 2 depicts the diffractograms of all the PtSn/C catalysts along with that of the Pt/C one. The reflections of the fcc structure of

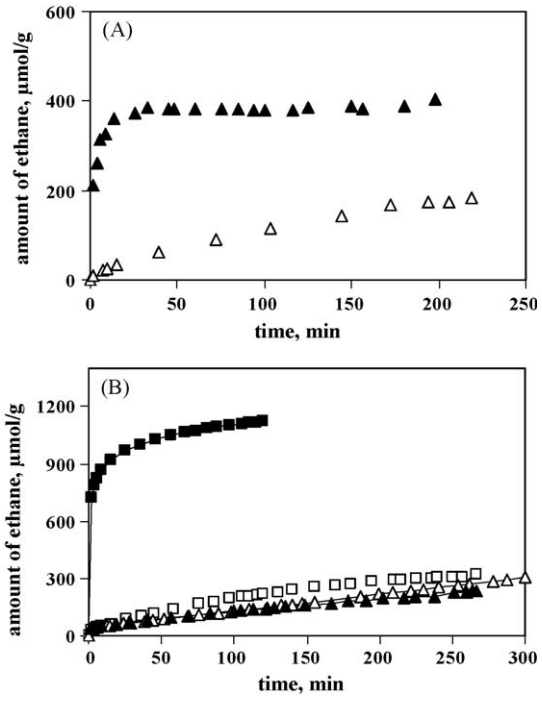

Fig. 1. Kinetic curves of the formation of ethane in tin anchoring step (1). (A) Preparation of PtSn-L catalyst. Periods of tin anchoring: (▲) period 1; (△) period 2. Conditions of tin anchoring: Sn_0/Pt = 0.5; T_r = 70 °C, new portion of H_2 was added at the beginning in each period, no further tin was introduced in period 2. (B) Preparation of PtSn-H catalyst. Periods of tin anchoring: (■) period 1; (□) period 2; (△) period 3; (▲) period 4. Conditions of tin anchoring: T_r = 120 °C, new portion of $Sn(C_2H_5)_4$ (Sn_0/Pt = 0.9) and H_2 was added at the beginning of each period.

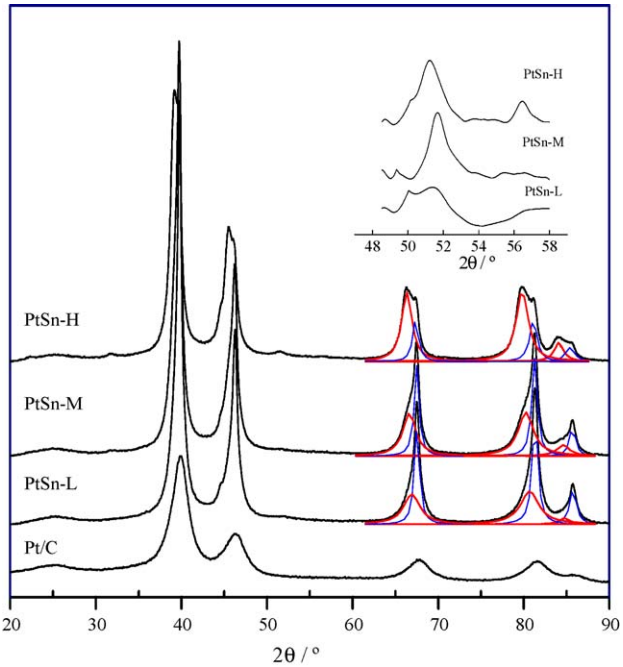

Fig. 2. XRD pattern of PtSn/C electrocatalysts. Contribution due to reflections ascribed to fcc $Pt_{1-x}Sn_x$ and Pt_3Sn are depicted in blue and red lines respectively. The inset shows a magnification of the superlattice reflections of the Pt_3Sn. (For interpretation of the references to color in this figure legend, the reader is referred to the web version of the article.)

Table 2
Particle size and lattice parameters of the Sn modified Pt/C catalysts determined from TEM and XRD analyses, respectively.

Catalyst	Size (nm) TEM	Pt rich phase	Sn rich phase
		Lattice parameter (Å)	Lattice parameter (Å)
Pt/C	–	3.915 ± 0.008	–
PtSn-L	5.5	3.920 ± 0.006	3.95 ± 0.02
PtSn-M	6.5	3.926 ± 0.001	3.964 ± 0.005
PtSn-H	5.6	3.932 ± 0.006	3.988 ± 0.008

[a]Pt lattice parameter = 3.9231 Å (PDF#04-0802). [b]Pt_3Sn lattice parameter = 4.0015 Å (PDF#35-1360).

platinum are the only ones observed. Noticeably, a shifting of the peaks to lower 2θ values with increasing tin loading is observed. This feature is in good agreement with the incorporation of tin into the fcc structure of platinum. Since the atomic radius of tin is larger than that of platinum, an expansion of the unit cell according to Vegard's law should be expected. The calculated values range between that of Pt (3.9231 Å) and Pt_3Sn (4.0015 Å) are summarized in Table 2. As evidenced from the XRD patterns depicted in Fig. 2, not only peaks shifted to lower 2θ values, but a second set of peaks at lower 2θ values appears as the Sn content increases. Each set of peaks correspond to Pt_3Sn (at lower 2θ) and $Pt_{1-x}Sn_x$ (at higher 2θ) phases, see Fig. 2 for further details. A careful deconvolution of XRD peaks at higher 2θ values of each phase allows calculation of the parameters of the Pt-rich ($Pt_{1-x}Sn_x$) and Sn-rich lattices. For the sake of comparison, the lattice parameter of the reference Pt/C catalyst was also calculated as shown in Table 2. It can be seen how the lattice parameter of the Sn-modified samples is larger than that of Pt/C. This applies both to Sn-rich and Pt-rich phases and it is in good agreement with the incorporation of Sn into the Pt lattice. The lattice parameter of the Sn-rich phase of the PtSn/C electrocatalysts becomes closer to that of Pt_3Sn as the Sn loading increases. A near-stoichiometric Pt_3Sn phase (a = 3.988 Å) is found for PtSn-H [30]. The lattice parameter derived from the Sn-rich reflections of PtSn-M and PtSn-L samples could reflect the presence of a certain amount of the $Pt_{90}Sn_{10}$ phase whose lattice parameter is a = 3.934 Å, or a lower amount of Sn in the Pt sublattice [31]. Furthermore, superlattice reflections ascribed to the Pt_3Sn phase are also observed in the diffractograms, those corresponding to 210 and 211 peaks being depicted in the inset to Fig. 2. In line with previous discussion, the intensity of these reflections increases with the tin loading, following the order PtSn-L ≪ PtSn-M < PtSn-H.

The diffractograms of the different samples reveal that $Pt_{1-x}Sn_x$ and Pt_3Sn are the only crystalline phases in the samples. Reflections that could be assigned to either PtSn phases other than above mentioned phases or Sn oxides were not found. Whereas the lack of Sn oxide species on similar carbon supported PtSn samples has been reported [30] however, other authors report the presence of tin oxides [15,31].

TEM images of the PtSn samples are depicted in Fig. 3. Mean particle sizes were determined by counting more than 2000 particles from different regions of each sample. Histograms displaying particle size distribution of the different samples are shown in the inset to the corresponding micrographs in Fig. 3(left). It can be observed that Sn incorporation results in an increase of the particle size from ca. 4.4 nm for Pt/C to 5.5–6.5 nm for the ones containing Sn. Particle size values as determined from TEM experiments are given in Table 2. From the low magnification micrographs a good dispersion of the metal particles on the carbon support in all samples is deduced. It can also be observed, as highlighted in Fig. 3b, that the nanoparticles are well crystallized generally exhibiting cuboctahedral or Wulff shape [32,33].

In line with previous analyses, no evidence of the presence of other alloyed PtSn phases is found from this type of study. Therefore, the shifting of the value of the lattice parameter of samples PtSn-L and PtSn-M with respect of the expected for pure Pt_3Sn phases is a consequence of the formation of non-stoichiometric $Pt_{1-x}Sn_x$ phases [34] rather than to the presence of the $Pt_{90}Sn_{10}$ phase.

EDX analysis (images not shown) of different regions of the samples reveals the coexistence of Pt particles along with Sn modified Pt particles with an average Sn composition of 12 ± 6, 17 ± 8 and 18 ± 6 at.% for PtSn-L, PtSn-M and PtSn-H, respectively. No evidence of Sn segregation was found. The EDX analysis of individual particles was possible by operating the microscope in the STEM mode. By focusing the beam in the Sn modified particles a 25 at.% composition of tin was found, in line the proposed Pt_3Sn crystal phases.

In line with XRD results, no evidence of the presence of SnO_2 phases in the Sn modified Pt/C samples were found by means of the TEM analysis. The presence of PtSn alloyed phases other than Pt_3Sn was not found either.

The surface composition of the carbon supported PtSn samples was studied by means of XPS. To this end, C 1s, Pt 4f and Sn 3d core levels were analyzed; the most intense component of the former peak was set at 284.6 eV and used as internal reference. The relative abundance of the surface species are depicted in Table 3. The Pt 4f region was fitted into three doublets whose most intense Pt $4f_{7/2}$ peak appears at 71.5 eV, a binding energy value being assigned to Pt^0. The spectra are depicted in Fig. 4(left). Besides, all samples display a variable amount of oxidized Pt, both as Pt^{2+} and Pt^{4+}, as deduced from the Pt $4f_{7/2}$ peaks at about 73.0–74.0 eV, respectively. The presence of Pt oxide phases accounts to the interaction of Pt with the support and to air exposure [35,36]. A certain shifting to lower binding energy of the Pt core level as the Sn loading in the sample increases can be observed, see Fig. 4(left). Such shifting would be in good agreement with a charge transfer from tin to Pt [37]. Admittedly, the magnitude of the shifting, ca. 0.2–0.3 eV (see Table 3) is within the threshold of the experimental error of the XPS technique. Although this result *per se* cannot be taken as conclusive of such interaction it endorses major conclusions derived from TEM and XRD analyses. It is also important to remark that the Pt^0/Pt atomic ratio is similar in all Sn modified Pt/C samples; the actual values are given in Table 3.

The Sn 3d core level spectra of all Sn modified Pt/C samples show the major Sn $3d_{5/2}$ component of the doublet at 486.4 eV (see Fig. 4(right)). On the one hand, this binding energy value has been assigned to Sn oxides species [30]. On the other hand, other authors claim that when alloyed, Sn^0 species can appear at a binding energy value as high as 486.0 eV [38]. Thus, an unequivocal assignment of the Sn species in the samples is not possible, but in line with results discussed above the presence of Sn oxide phases is discarded. The Sn 3d core level spectra (depicted in Fig. 4(right)) display a FWMH of ∼1.9 eV in line with the presence of a single Sn species in the samples. As expected, as the Sn content in the samples is increased, the Pt/Sn atomic ratio decreases as observed from the XPS analysis. The most relevant data obtained from the XPS analysis are depicted in Table 3.

In summary, characterization data suggest that the incorporation of Sn to Pt/C was achieved satisfactorily yielding an intermetallic Pt_3Sn phase along with a minor contribution of $Pt_{1-x}Sn_x$. The amount of the Pt_3Sn phase prevails with increasing the tin content in the order PtSn-L < PtSn-M < PtSn-H. Neither XRD nor microscopy analyses reveal the presence of Sn oxides.

3.3. Electrochemical characterization

CO and ethanol electrooxidation was studied by means of electrochemical techniques. Fig. 5 depicts the voltammograms of the different electrocatalysts recorded in N_2 purged $HClO_4$ solutions at 10 mV/s. Previous to the oxidation studies, the Sn

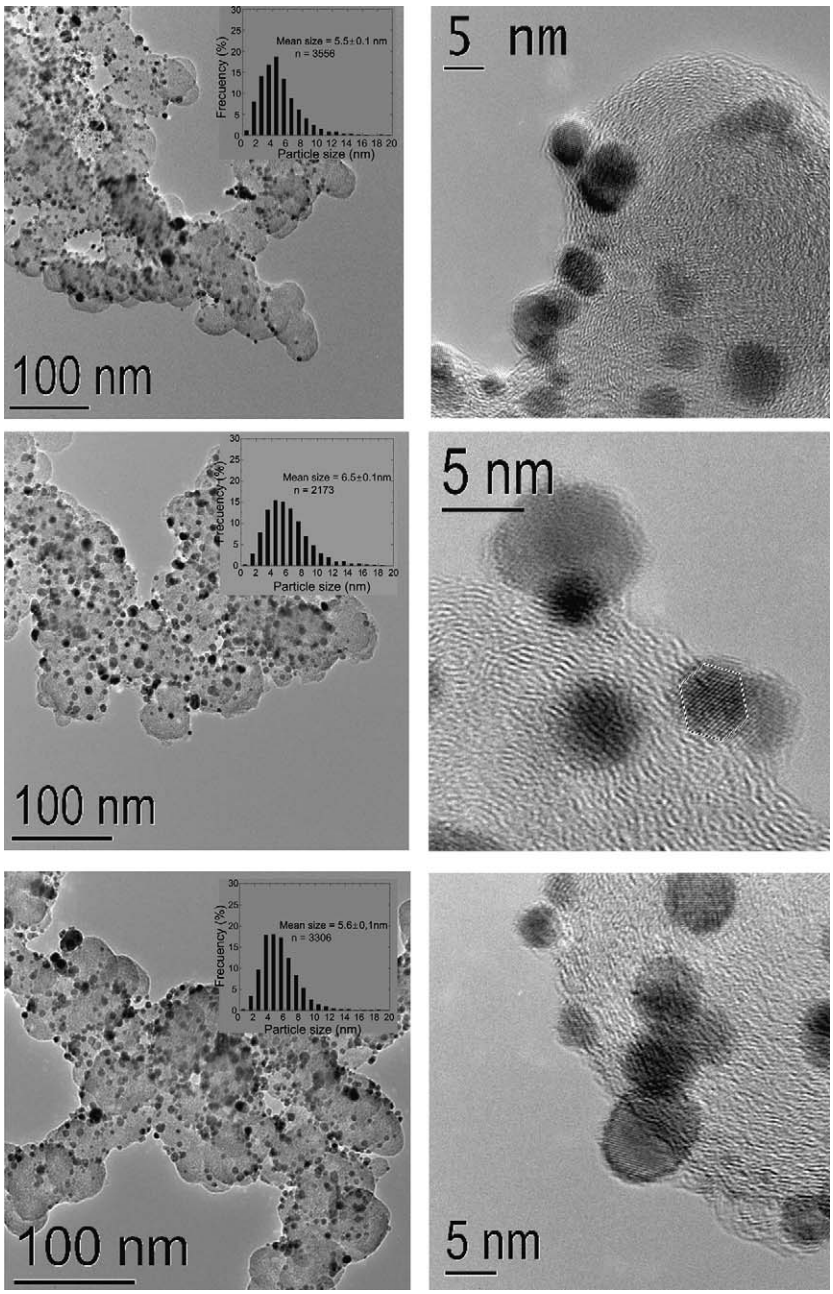

Fig. 3. A TEM (left) and HR-TEM (right) images and corresponding particle size distribution histograms (inset to a–c) for (a) PtSn-L, (b) PtSn-M and (c) PtSn-H.

Table 3
Nomenclature and characterization data of the Sn modified Pt/C samples.

Catalyst	Pt (wt.%)[a]	Sn (wt.%)[b]	Pt/Sn[c]	Pt^0/Pt[c]	Pt $4f_{7/2}$[d] B.E. (eV)
PtSn-L	40	1.9	2.4	48	71.5 (48) 72.9 (28) 74.5 (24)
PtSn-M	40	4.3	2.2	46	71.3 (45) 72.5 (34) 74.3 (21)
PtSn-H	40	6.2	2.0	50	71.3 (50) 72.4 (32) 74.0 (18)

[a] Pt content of the parent sample provided by the supplier.
[b] Sn wt.% determined from material balance of tin anchoring.
[c] Surface composition derived from XPS data.
[d] The binding energy of the Pt $4f_{7/2}$ core level of the Pt^0 species in parent Pt/C sample is 71.6 eV.

modified Pt/C electrocatalysts were subjected to a potential program of 10 consecutive cycles between 0.01 and 1.0 V at 100 mV/s until the profile of the *i*–*E* curve was invariable. The characteristic hydrogen adsorption/desorption features of Pt samples become ill-defined as the Sn content increases, see Fig. 5. This feature is well documented; see for instance reference [14]. The electroactive area of Pt (see Table 4) has been determined by integration of the hydrogen adsorption/desorption areas of the different PtSn/C samples. Due to the presence of Sn it is not a straightforward calculus and some authors are not prone to give those values [14] however, other authors actually prefer showing them [30]. For the sake of comparison, we have chosen to give the Pt area calculated from the hydrogen area; the values are depicted in Table 4.

The Pt oxide region is also modified by the presence of tin, the onset of the oxide formation region, and the oxygen reduction peak being shifted to less positive potentials as the Sn content increases

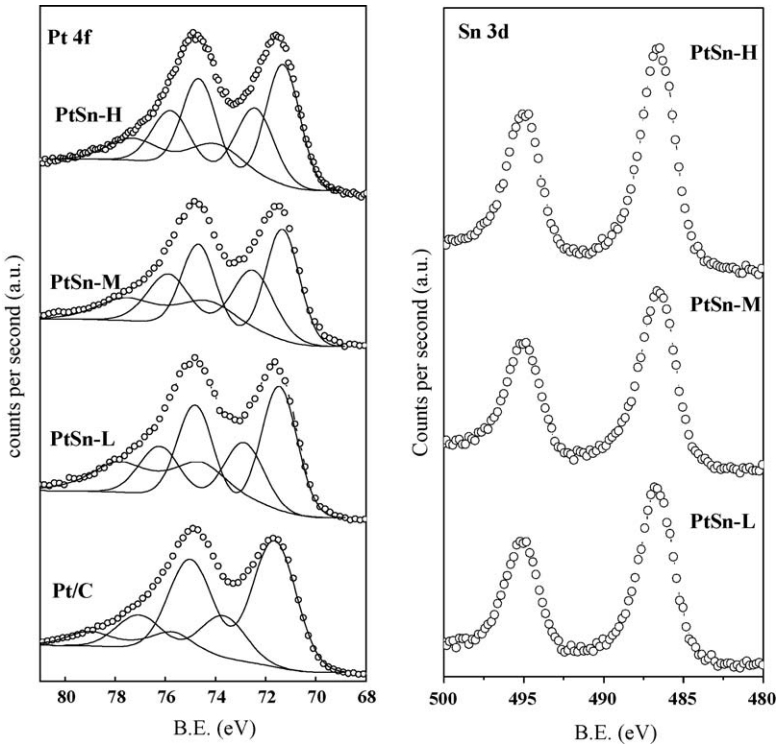

Fig. 4. XPS spectra of the Pt 4f (left) and Sn 3d (right) core levels of the Sn modified Pt/C samples.

(see Fig. 5). Noticeably, a single oxide reduction peak is observed in all samples. The peak is shifted to less positive potential values for the Sn containing samples. Although not reported explicitly, previous studies with PtSn electrodes displayed similar behavior [9,25]

3.4. CO and ethanol electrooxidation

CO oxidation reaction on Sn modified Pt/C sample was evaluated by means of the CO stripping technique. Briefly, CO is preadsorbed at constant potential of 20 mV during 15 min. Then, Ar is flown to remove dissolved CO during 45 min. Three consecutive potentials scans at 10 mV/s between 0 and 1 V were recorded. Even though Sn promoted Pt catalysts are known to oxidize CO at rather low potentials (less positive than bare Pt or even PtRu), the CO_{ad} layer cannot be fully removed at potentials less positive than 500 mV [14]. Therefore, in order to assure complete removal of CO_{ad}, reaching such positive potentials as 1.0 V is necessary. It has been previous evidenced that Sn dissolves during potential excursions more positive than 500 mV. In fact this process occurs in parallel to the CO oxidation impeding an accurate determination of the exposed surface area of Pt by means of the CO stripping technique [14]. On the contrary, other authors report that Sn, when alloyed with Pt, is stable at potentials at least upto 1.2 V [39]. Nevertheless, in line with the determination of the Pt surface area from the hydrogen adsorption/desorption area, this study is rather useful for comparing the performance amongst different samples. Furthermore, the onset potential of the CO electrooxidation reaction is a relevant parameter for the designing of CO tolerant electrocatalysts.

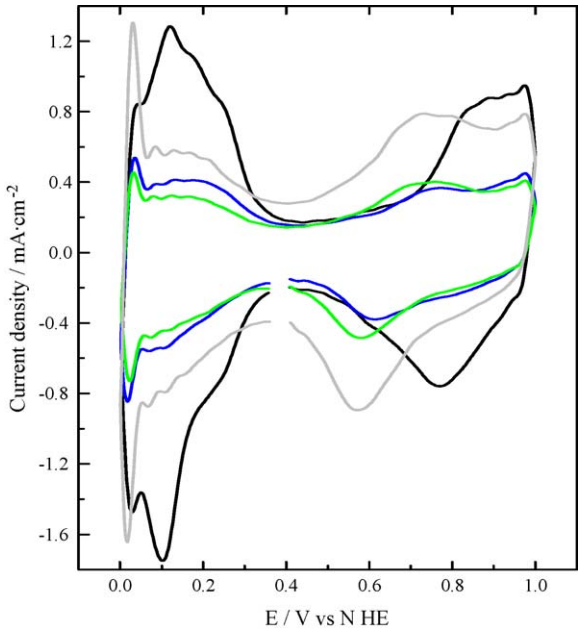

Fig. 5. Cyclic voltammogram of Pt/C (black), PtSn-L (blue), PtSn-M (green) and PtSn-H (grey) recorded in 0.5 M $HClO_4$ at 10 mV/s. (For interpretation of the references to color in this figure legend, the reader is referred to the web version of the article.)

The *i–E* plots recorded both on the parent Pt/C and Sn-Pt/C electrocatalysts with different Pt/Sn ratios during the CO oxidation process are depicted in Fig. 6A–D. It can be seen that during the CO stripping cycle (first cycle after CO admission) the hydrogen features are not observed, reflecting a blocking of the Pt sites due to the presence of adsorbed CO. It should be stated that on Pt_3Sn

Table 4
Pt area as determined from the hydrogen adsorption–desorption region. Electrocatalityc area (ECA) normalized to the amount of Pt determined from the CO stripping analysis. Current density of the ethanol electrooxidation on the different samples recorded in similar conditions at 450 mV, normalized to the ECA.

	Area (cm^2_{Pt})	ECA $\left(\frac{m^2_{Pt}}{gPt}\right)$	j_{450mv} (mA/cm^2)
PtSn-L	10.8	27.9	300
PtSn-M	10.2	26.3	580
PtSn-H	15.0	38.6	660

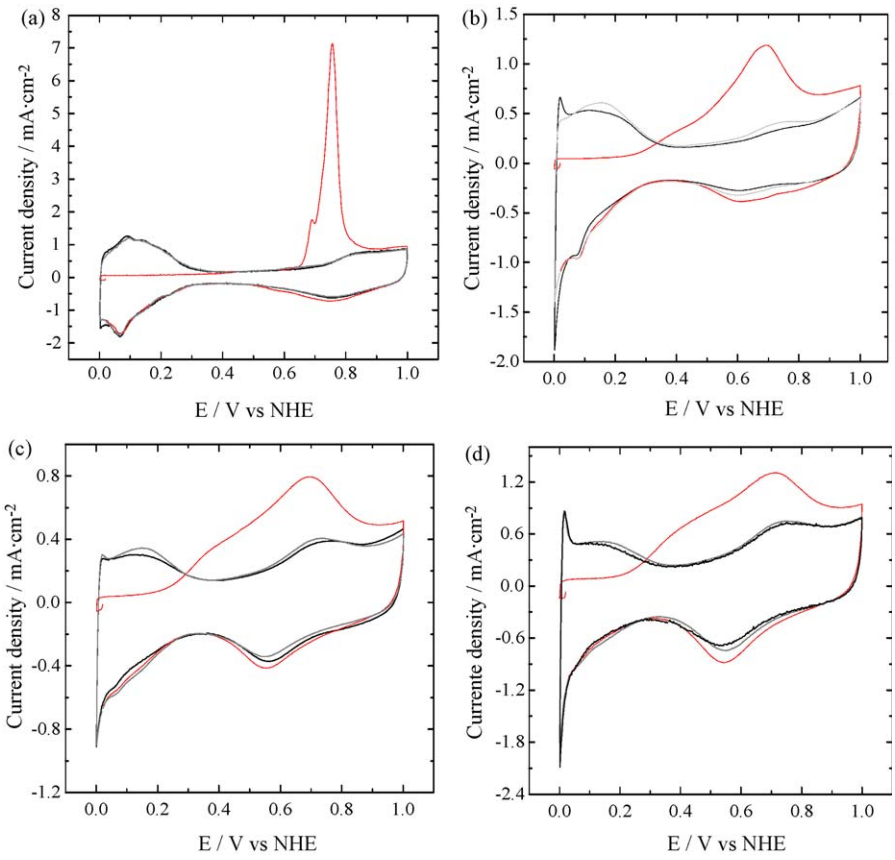

Fig. 6. CO oxidation (stripping analysis) (red line) on fresh catalysts: Pt/C (a), PtSn-L (b), PtSn-M (c) and PtSn-H (d) at 10 mV/s in 0.5 M HClO4. The cycles recorded before and after the CO oxidation process are depicted in black and grey respectively. (For interpretation of the references to color in this figure legend, the reader is referred to the web version of the article.)

surfaces CO is adsorbed exclusively on the Pt sites [40]. The hydrogen features are clearly observed during the reverse and successive scans. In fact the hydrogen profile is identical to that recorded previous to CO adsorption. This feature illustrates the stability of the samples during the process. The onset potential ($E_{co,onset}$) for the oxidation of CO on Pt/C, PtSn-L, PtSn-M and PtSn-H is 620, 300, 220 and 210 mV, respectively. In line with previous works, it can be seen that the presence of Sn promotes CO electrooxidation compared to bare Pt catalysts. Other groups reported comparable values for the onset of the CO oxidation on similar samples [9,15,25]. It is also documented that CO oxidation on PtSn catalysts obey a bifunctional mechanism in which CO is adsorbed on Pt whereas, Sn sites nucleate OH_{ad} species at less positive potentials than Pt [41–42]. Furthermore, it has been reported that CO oxidation is a structure-sensitive reaction, being favored on the Pt_3Sn (1 1 1) surface [14,40]. Remarkably, the results shown here not only show how the presence of Sn favors the CO oxidation reaction, but it highlights the importance of the Pt_3Sn phase in the CO electrooxidation reaction. In fact, PtSn-H containing a larger amount of this intermetallic phase (see XRD data) oxidizes CO at the less positive potential in the series. Nonetheless, a strong promotion of the CO oxidation process is observed even on PtSn-L when compared to Pt/C. Fig. 6 illustrates, how the positive current ascribed to the CO oxidation process (straight red line) on PtSn-L occurs within the potential region where oxide species are formed. In fact, the standard redox potentials of the Sn/Sn^{2+} and Sn^{2+}/Sn^{4+} couples are −0.13 and +0.15 V *vs* SHE, respectively [43]. This result is in good agreement with previous discussion in the sense that CO oxidation on PtSn samples is promoted due to the formation of $Sn–OH_{ad}$ species.

When it comes to the oxidation of ethanol the picture is not fully understood whereas, some studies report the beneficial effect of the formation of PtSn alloy other studies conclude that pure Pt integrated with tin oxide will suffice for the efficient ethanol electrooxidation [43].

The performance of the Sn modified Pt/C samples as ethanol electrooxidation catalysts has been evaluated by comparing two key parameters: (i) the onset potential of ethanol electrooxidation and (ii) the current density obtained at selected potentials. Fig. 7 collects the results obtained during ethanol electrooxidation. The onset potential values for ethanol electrooxidation ($E_{EtOH,\ onset}$) are: 310, 160, 120 and 100 mV for Pt/C, PtSn-L, PtSn-M and PtSn-H, respectively. To the best of our knowledge, these are the best results published for the oxidation of ethanol. Values as low as either 250 mV [16] or 200 mV [9,44,45] being amongst the best results reported. Furthermore, the onset potential on PtSn-M and PtSn-H was set as to that value where the oxidation current surpasses that of the hydrogen desorption region. A careful inspection of the voltammograms reveals that the ethanol electrooxidation process actually begins at less positive potentials. It is obvious that the presence of the Pt_3Sn phase promotes the oxidation of ethanol to a great extent. More importantly, a direct relationship between the amount of Pt_3Sn and the electrooxidation of ethanol can be established.

The current density (normalized to the actual Pt area derived from the hydrogen adsorption/desorption values) for the ethanol oxidation process on the different electrodes at 450 mV has been compared in Table 4. Clearly, the electrooxidation process increases as the amount of Pt_3Sn phase increases. The comparison is clearly illustrated in Fig. 8 where a magnification of the forward

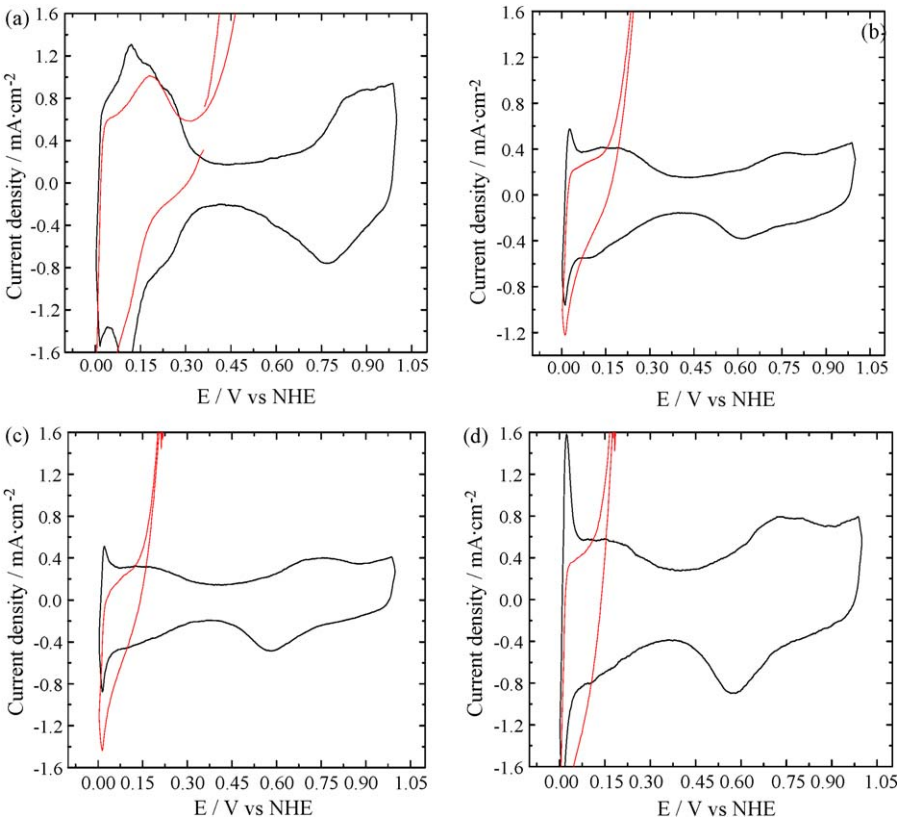

Fig. 7. Ethanol electrooxidation (red lines) on Pt/C (a), PtSn-L (b), PtSn-M (c) and PtSn-H (d) recorded at 10 mV/s in 0.5 M CH_3CH_2OH/ 0.5 M $HClO_4$. Base voltammograms are depicted as straight lines. (For interpretation of the references to color in this figure legend, the reader is referred to the web version of the article.)

scan of the ethanol electrooxidation reaction on the different electrodes is depicted. The magnitude of the oxidation current increases in the order: PtSn-L < PtSn-M ≪ PtSn-H. The potential onset for the ethanol electrooxidation reaction follows the order: PtSn-H < PtSn-M < PtSn-L.

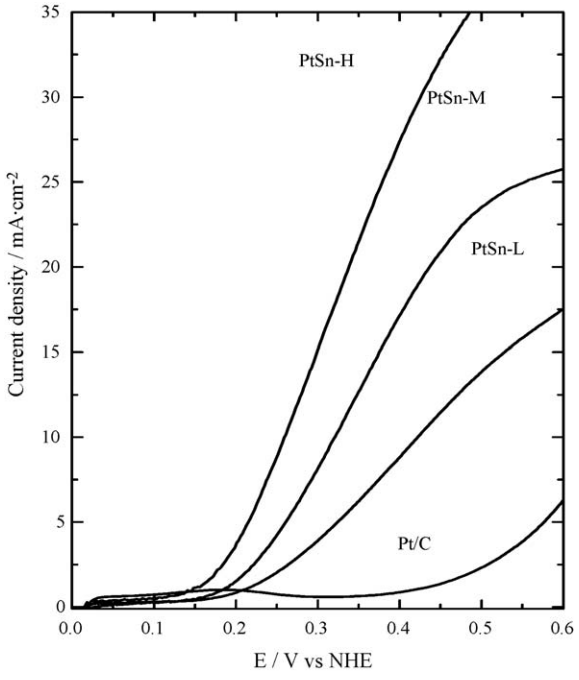

Fig. 8. Ethanol electroxidation on Pt/C, PtSn-L, PtSn-M and PtSn-H recorded in 0.5 M CH_3CH_2OH/0.5 M $HClO_4$ at 10 mV/s.

Ethanol electrooxidation to CO_2 is a complex reaction involving successive dehydrogenation steps to form adsorbed CO [9]. Early stages of ethanol electrooxidation, which imply a dehydrogenative adsorption on Pt, can take place either through the C or the O atoms [46,47], see Eqs. (3) and (4). However, due to the difficulty in breaking the C–C bond, the main oxidation products obtained are acetaldehyde (AAL) and acetic acid (AA), particularly for Pt/C catalysts [9]. Furthermore, even on PtSn/C or PtRu/C catalysts the yielding to CO_2 (complete oxidation) is rather low, below 2% as reported in [44]. On the other hand, as discussed previously, for the oxidation of CO (complete oxidation of ethanol) $Sn–OH_{ad}$ species are necessary, see Eq. (5).

$$Pt + CH_3–CH_2OH \rightarrow Pt–OCH_2–CH_3 + e^- + H^+ \quad (3)$$

$$Pt + CH_3–CH_2OH \rightarrow Pt–CHOH–CH_3 + e^- + H^+ \quad (4)$$

$$Pt + CO_{ad} + Sn–OH_{ad} \rightarrow CO_2 + e^- + H^+ \quad (5)$$

According to the bifunctional mechanism [48], the role of tin (or other oxophilic metals such as Ru) consists in activating water to form OH_{ad} species at less positive potentials than Pt, thus favoring the CO oxidation reaction. As discussed above, ethanol electrooxidation is far from complete. In fact, at low potentials, say <250 mV, ethanol dehydrogenation steps are responsible of the positive current in the voltammograms. In principle and according to reactions (3) and (4), $Sn–OH_{ad}$ species, even if already formed, are not expected to play a major role in the ethanol dehydrogenation process. Rather, geometry or electronic factors (or both) will dominate adsorption and dehydrogenation of ethanol onto the active sites. Spectroscopic results show how bimetallic electrocatalysts (PtSn and PtRu) adsorb ethanol at lower potentials than bare Pt ones [49]. This process could be related to the downward d-band shift of Pt in the Pt_3Sn structure [41] weakening ethanol

adsorption or by a larger intermetallic distance of the atoms in the Pt_3Sn network. The actual nature of the promotional effect of the Pt_3Sn phase in the early stages of the ethanol electrooxidation is out of the scope of this paper. However, results shown in this manuscript clearly illustrate how the Pt_3Sn phase improves the performance of Pt in this early stages of the ethanol electrooxidation reaction, particularly within the potential range <200 mV. At more positive potentials, the facile nucleation of $Sn–OH_{ad}$ promotes the oxidation of CO as depicted in Eq. (5).

4. Conclusions

Controlled surface reactions between $Sn(C_2H_5)_4$ and Pt/C result in the formation of carbon supported intermetallic Sn modified Pt electrocatalyst. The incorporation of Sn results in the exclusive formation of intermetallic $Pt_{1-x}Sn_x$ and Pt_3Sn phases as demonstrated by XRD and microscopy analyses. The amount of the Pt_3Sn phase can be tuned by using the appropriate reaction conditions. It was demonstrated that the formation of Pt_3Sn intermetallic phase can substantially be increased under following experimental conditions: (i) high reaction temperature (T_r = 120 °C), (ii) high Sn_o/Pt ratio, and (iii) the use of several consecutive tin anchoring periods.

The new type of PtSn/C electrocatalysts were tested in both CO and ethanol electrooxidation reactions. The performance of the samples in either reaction depended on the amount of the Pt_3Sn phase. As the amount of Pt_3Sn phase increases in a sample its performance towards CO and ethanol oxidation is better both in terms of onset potential of the oxidation reaction (shifted to more negative values) or current density. The superior CO oxidation ability can be ascribed to the facile formation of $Sn–OH_{ad}$, occurring at less positive potentials than Pt alone. On the other hand, ethanol electrooxidation is favored over Pt_3Sn phase due to factors such as the enlargement of the Pt–Pt bond in the Pt_3Sn network and downward of d-band center after alloying with Sn.

Acknowledgements

Spain's Ministry of Science and Education is acknowledged for the financial support provided by project ENE2007-67533-C02-01. S. Rojas acknowledges project 200780I017 for support. S. García acknowledges the fellowship provided by the I3P Program co-funded by the European Social Fund. Project MTA-CSIC/2007–2008 (no. 06) is also acknowledged for financial support.

References

[1] C. Lamy, A. Lima, V. LeRhum, F. Delime, C. Coutanceau, J.-M. Léger, J. Power Sources 105 (2002) 283–296.
[2] S. Rousseau, C. Coutanceau, C. Lamy, J.-M. Léger, J. Power Sources 158 (2006) 18–24.
[3] S. Song, Y. Wang, P. Shen, Chin. J. Catal. 28 (2007) 752–754.
[4] N.M. Markovic, P.N. Ross, Cattech 4 (2000) 110–126.
[5] S. Song, P. Tsiakaras, Appl. Catal. B: Environ. 63 (2006) 187–193.
[6] W.J. Zhou, W.Z. Li, S.Q. Song, Z.H. Zhou, L.H. Jiang, G.Q. Sun, Q. Xin, K. Poulianitis, S. Kontou, P. Tsiakaras, J. Power Sources 131 (2004) 217–223.
[7] C. Lamy, S. Rousseau, E.M. Belgsir, C. Coutanceau, J.-M. Léger, Electrochim. Acta 49 (2004) 3901–3908.
[8] E. Antolini, J. Power Sources 170 (2001) 1–12.
[9] F. Vigier, C. Countanceau, F. Hahn, E.M. Belgsir, C. Lamy, J. Electroanal. Chem. 563 (2004) 81–89.
[10] W. Zhou, Z. Zhou, S. Song, W. Li, G. Sun, P. Tsiakara, Q. Xin, Appl. Catal. B: Environ. 46 (2003) 273–285.
[11] V.R. Stamenković, M. Arenz, C.A. Lucas, M.E. Gallagher, P.N. Ross, N.M. Marković, J. Am. Chem. Soc. 125 (2003) 2736–2745.
[12] S. Pick, Surf. Sci. 436 (1999) 220–226.
[13] S. Speller, U. Bardi, in: D.P. Woodruff (Ed.), The Chemical Physics of Solid Surfaces, Surface Alloys and Alloy Surfaces, vol. 10, Elsevier, 2002 (Chapter 4).
[14] M. Arenz, V. Stamenković, B.B. Blizanac, K.J. Mayrhofer, N.M. Marković, P.N. Ross, J. Catal. 232 (2005) 402–410.
[15] Z. Liu, D. Reed, G. Kwon, M. Shamusuzzoha, D.E. Nikles, J. Phys. Chem. C 111 (2007) 14223–14229.
[16] L. Jiang, Z. Zhou, W. Li, W. Zhou, S. Song, H. Li, G. Sun, Q. Xin, Energy Fuels 28 (2004) 866–871.
[17] L. Colmenares, H. Wang, Z. Jusys, L. Liang, S. Yan, G.Q. Sun, R.J. Behm, Electrochim. Acta 52 (2006) 221–233.
[18] F. Colmati, E. Antolini, E.R. Gonzalez, Electrochim. Acta 50 (2005) 5496–5503.
[19] Y. Wang, J.Y. Lee, T.C. Deivaraj, J. Mater. Chem. 14 (2004) 362–365.
[20] G.J. Siri, J.M. Ramallo-López, M.L. Casella, J.L.G. Fierro, F.G. Requejo, O.A. Ferretti, Appl. Catal. A: Gen. 278 (2005) 239–249.
[21] N. Kamiuchi, T. Matsui, R. Kikuchi, K. Eguchi, J. Phys. Chem. C 111 (2007) 16470–16476.
[22] J.L. Margitfalvi, I. Borbáth, E. Tfirst, A. Tompos, Catal. Today 43 (1998) 29–49.
[23] J.L. Margitfalvi, I. Borbáth, K. Lázár, E. Tfirst, A. Szegedi, M. Hegedűs, S. Gőbölös, J. Catal. 203 (2001) 94–103.
[24] J.L. Margitfalvi, I. Borbáth, M. Hegedűs, E. Tfirst, S. Gőbölös, K. Lázár, J. Catal. 196 (2000) 200–204.
[25] E.M. Crabb, R. Marshall, D. Thompsett, J. Electrochem. Soc. 147 (2000) 4440–4447.
[26] J. Margitfalvi, S. Szabó, F. Nagy, in: L. Cerveny (Ed.), Catalytic Hydrogenation, Stud. Surf. Sci. Catal., vol. 27, Elsevier, Amsterdam, 1986, p. 373.
[27] J.L. Margitfalvi, E. Tálas, S. Gőbölös, Catal. Today 6 (1989) 73–80.
[28] P. Hernández-Fernández, S. Rojas, P. Ocón, A. de Frutos, J.M. Figueroa, P. Terreros, M.A. Peña, J.L.G. Fierro, J. Power Sources 177 (2008) 9–16.
[29] J.L. Margitfalvi, I. Borbáth, M. Hegedűs, A. Tompos, Appl. Catal. 229 (2002) 35–49.
[30] J.H. Kim, S.M. Choi, S.H. Nam, M.H. Seo, S.H. Choi, W.B. Kim, Appl. Catal. B: Environ. 82 (2008) 89–102.
[31] V. Radmilovic, T.J. Richardson, S.J. Chen, P.N. Ross Jr., J. Catal 232 (2005) 199–209.
[32] G. Wulff, Z. Krystallorg, Mineral 34 (1901) 499–530.
[33] C.R. Henry, Prog. Surf. Sci. 80 (2005) 92–116.
[34] I.R. Harris, M. Norman, A.W. Bryant, J. Less Common Met. 16 (1968) 427–440.
[35] E. Antolini, Mat. Chem. Phys. 78 (2003) 563–573.
[36] J.L. Gómez de la Fuente, S. Rojas, M.V. Martínez-Huerta, P. Terreros, M.A. Peña, J.L.G. Fierro, Carbon 44 (2006) 1919–1929.
[37] A.S. Aricò, V. Antonucci, N. Giordano, A.K. Shukla, M.K. Ravikumar, A. Roy, S.R. Barman, D.D. Sarma, J. Power Sources 50 (1994) 295–309.
[38] M.M. Schubert, M.J. Kahlich, G. Feldmeyer, M. Hüttner, S. Hackenberg, H.A. Gasteiger, R.J. Behm, Phys. Chem. Chem. Phys. 3 (2001) 1123–1131.
[39] S. Szabó, J. Electroanal. Chem. 172 (1984) 359–366.
[40] V. Stamenković, M. Arenz, B.B. Blizanac, K.J.J. Mayrhofer, N.M. Marković, P.N. Ross, Surf. Sci. 576 (2005) 145–157.
[41] P. Liu, A. Logadottir, J.K. Norskov, Electrochim. Acta 48 (2003) 3737–3742.
[42] M.T.M. Koper, Surf. Sci. 548 (2004) 1–3.
[43] J. Mann, N. Yao, A.B. Cocarsly, Langmuir 22 (2006) 10432–10436.
[44] H. Wang, Z. Jusys, R.J. Behm, J. Power Sources 154 (2006) 351–359.
[45] L. Jiang, L. Colmenares, Z. Jusys, G.Q. Sun, R.J. Behm, Electrochim. Acta 53 (2007) 377–389.
[46] T. Iwasita, E. Pastor, Electrochim. Acta 39 (1994) 531–537.
[47] T. Iwasita, E. Pastor, Electrochim. Acta 39 (1994) 547–551.
[48] T. Yajima, H. Uchida, M. Watanabe, J. Phys. Chem. B 108 (2004) 2654–2659.
[49] Q. Wang, G.Q. Sun, L.H. Jiang, Q. Xing, S.G. Sun, Y.X. Jiang, S.P. Chen, Z. Jusys, R.J. Behm, Phys. Chem. Chem. Phys. 9 (2007) 2686–2696.